2008

# Reaction mechanism of the direct gas phase synthesis of H2O2 catalyzed by Au3

Bosiljka Njegic
*Iowa State University*

Mark S. Gordon
*Iowa State University*, mgordon@iastate.edu

# Reaction mechanism of the direct gas phase synthesis of H2O2 catalyzed by Au3

**Abstract**
The gas phase reaction of molecular oxygen and hydrogen catalyzed by a Au3cluster to yield H2O2 was investigated theoretically using second order Z-averaged perturbation theory, with the final energies obtained with the fully size extensive completely renormalized CR-CC(2,3) coupled clustertheory. The proposed reaction mechanism is initiated by adsorption and activation of O2 on the Au3cluster. Molecular hydrogen then binds to the Au3O2 global minimum without an energy barrier. The reaction between the activated oxygen and hydrogen molecules proceeds through formation of hydroperoxide (HO2) and a hydrogen atom, which subsequently react to form the product hydrogen peroxide. All reactants, intermediates, and product remain bound to the goldcluster throughout the course of the reaction. The steps in the proposed reaction mechanism have low activation energy barriers below 15kcal⁄mol. The overall reaction is highly exothermic by ~30kcal⁄mol.

**Keywords**
Gold, Hydrogen reactions, Activation energies, Reaction mechanisms, Density functional theory

**Disciplines**
Chemistry

**Comments**
The following article appeared in *Journal of Chemical Physics* 129 (2008): 124705, and may be found at doi:10.1063/1.2977967.

# Reaction mechanism of the direct gas phase synthesis of H 2 O 2 catalyzed by Au 3

Bosiljka Njegic and Mark S. Gordon

Citation: The Journal of Chemical Physics **129**, 124705 (2008); doi: 10.1063/1.2977967
View online: http://dx.doi.org/10.1063/1.2977967
View Table of Contents: http://scitation.aip.org/content/aip/journal/jcp/129/12?ver=pdfcov
Published by the AIP Publishing

# Reaction mechanism of the direct gas phase synthesis of $H_2O_2$ catalyzed by $Au_3$

Bosiljka Njegic and Mark S. Gordon[a)]
*Department of Chemistry, Iowa State University, Ames, Iowa 50011, USA*

(Received 20 May 2008; accepted 12 August 2008; published online 24 September 2008)

The gas phase reaction of molecular oxygen and hydrogen catalyzed by a $Au_3$ cluster to yield $H_2O_2$ was investigated theoretically using second order *Z*-averaged perturbation theory, with the final energies obtained with the fully size extensive completely renormalized CR-CC(2,3) coupled cluster theory. The proposed reaction mechanism is initiated by adsorption and activation of $O_2$ on the $Au_3$ cluster. Molecular hydrogen then binds to the $Au_3O_2$ global minimum without an energy barrier. The reaction between the activated oxygen and hydrogen molecules proceeds through formation of hydroperoxide ($HO_2$) and a hydrogen atom, which subsequently react to form the product hydrogen peroxide. All reactants, intermediates, and product remain bound to the gold cluster throughout the course of the reaction. The steps in the proposed reaction mechanism have low activation energy barriers below 15 kcal/mol. The overall reaction is highly exothermic by ~30 kcal/mol. © *2008 American Institute of Physics*. [DOI: 10.1063/1.2977967]

## INTRODUCTION

Propylene oxide is an important bulk chemical used for production of mainly polyether polyols, propylene glycol, and glycol ethers. Thus, manufacturing of propylene oxide is a very important industrial process, currently mainly achieved by the oxidation of propylene using chlorohydrin or hydrogen peroxide methods.[1] Chlorohydration involves oxidation of propylene by chlorine in the presence of lime and leads to the production of chlorinated organic by-products that are pollutants and as such difficult to dispose of properly. In addition, huge quantities of $CaCl_2$ that do not have any practical use but also need to be disposed of are produced. On the other hand, hydrogen peroxide processes are carried out using organic peroxides, mainly derived from isobutene and ethylbenzene, which yield useful coproducts, such as *t*-butanol (a gasoline additive) and 1-phenyl ethanol that can be dehydrated to styrene and subsequently polymerized into the important synthetic material polystyrene. However, epoxide production by this approach is not yet cost effective.

Hydrogen peroxide might be a natural choice of oxidant for the epoxidation of propene; however, an effective catalyst is needed. Although the catalytic activity of gold was recognized as early as the 1980s,[2] an important breakthrough came through the work of Kalvachev *et al.*[3] in the mid-1990s. These authors demonstrated that gold nanoparticles supported on titanium silicates catalyze the epoxidation of propene by hydrogen peroxide species formed *in situ* from gaseous hydrogen and oxygen. Recently several companies have developed a new approach[4] in which hydrogen peroxide is used as an oxidant, thus making the production of propylene oxide a green industrial process since the by-product is water.

A very nice review on the epoxidation of propene by Min and Friend[5] also noted that although the propene epoxidation mechanism is still under investigation, a hydrogen peroxolike species is the likely oxidant. This assertion is supported by the known effective epoxidation of propene by hydrogen peroxide promoted by titania catalysts.[6] Furthermore, it has been confirmed experimentally that hydrogen peroxide[7] and peroxide species[8] are formed from $H_2$ and $O_2$ in the reaction catalyzed by gold supported on titania. However, there is as yet no experimental evidence for the existence of peroxide species during the epoxidation reaction involving $H_2$ and $O_2$. An issue that is related to the mechanism of hydrogen peroxide formation from $H_2$ and $O_2$ over gold catalysts is that hydrogen peroxide production currently takes place through sequential hydrogenation and oxidation of an alkyl anthraquinone.[1] This method is limited by the cost of the solvent, the necessity of periodic replacement of the catalyst due to hydrogenation, and the large scale of the production. This last point further increases the cost because of the risks related to transportation and storage of the produced hydrogen peroxide.

A recent study by Nijhuis *et al.*[9] suggests a possible explanation for the aforementioned lack of experimental evidence for peroxide. According to their proposed mechanism, the reaction proceeds though the binding of propene to titania to produce a propoxy species, which then gets desorbed from the catalyst by a peroxide species to form epoxide and water. If the formation of the peroxide species is indeed the rate-controlling step of the epoxidation reaction, then one may infer that the concentration of this intermediate will stay below the sensitivity of detection throughout the reaction. However, a theoretical study[10] carried out with density functional theory (DFT) suggests that the epoxidation of propene is the rate-controlling step, with an activation energy of 19.6 kcal/mol, while the formation of the peroxide species

[a)]Electronic mail: mark@si.msg.chem.iastate.edu.

 

requires only 2.2 kcal/mol. Therefore, further theoretical work is needed to help resolve the discrepancy between experimental data and theoretical predictions.

The intent of the work presented in this paper is to shed additional light on the mechanism of the $H_2/O_2$ reaction catalyzed by a $Au_3$ cluster to form an intermediate hydroperoxide, a possible oxidant in the epoxidation reaction, and the final product, hydrogen peroxide, an important oxidant under mild conditions. The size of the gold cluster was chosen based on two factors. The number of gold atoms needs to be reasonably small, so accurate *ab initio* calculations, such as perturbation theory and coupled cluster theory, can be employed. On the other hand, the gold cluster needs to be large enough to bind both $O_2$, which prefers to bind to clusters with an odd number of electrons,[11,12] and $H_2$, which does not bind to negatively charged clusters.[13] Hence, $Au_3$ is the simplest useful gold cluster to model $H_2O_2$ formation. Activation energy barriers and the overall reaction enthalpy are reported.

## COMPUTATIONAL DETAILS

Geometry and saddle point optimizations,[14] Hessians (energy second derivatives),[15] and intrinsic reaction paths[16] are calculated with (spin-correct) *Z*-averaged second order perturbation theory (ZAPT).[17] All stationary points are tightly optimized, with the largest component of the analytic gradient[18] being smaller than $10^{-5}$ hartree/bohr. Hessian calculations were obtained seminumerically using double differencing of analytic gradients.

The general approach used for locating transition states was to create a linear least motion (LLM) path, determined by linear interpolation between the coordinates of the two corresponding minima. Single point energy calculations were performed at each LLM point. This was followed by constrained optimizations at each of these points, thereby creating a linear synchronous transit (LST) path. The structure with the highest energy on the LST path is then chosen as the starting point for locating the transition state. The optimized geometries for all stationary points were used to do single point energy calculations with restricted open shell completely renormalized left eigenvalue singles and doubles coupled cluster theory with perturbative triples, CR-CCSD(T)$_L$.[19] The CR-CCSD(T)$_L$ [or equivalently CR-CC(2,3)] method is size extensive and has been shown to break single bonds correctly for both open and closed shell species.[20] The shorthand notation used here for this method is CCL. These CCL energies were then used to calculate more accurate energy barriers ($\Delta E_b$) and activation energies ($\Delta E_a$), which include zero point energy (ZPE) corrections, calculated with the harmonic approximation without frequency scaling, and thermal corrections to 425 K. The latter temperature was chosen based on the experimental conditions for the epoxidation reaction.[21] The apparent energy of activation [$\Delta E_a$(app)] is calculated as the difference in the energy of the highest transition state and the reactants. Binding energies ($\Delta E_{\text{bind}}$) are calculated as the difference between the energy of the product and the sum of the energies of the separated species. The reaction enthalpy ($\Delta H_r$) represents the difference in the enthalpies of the product and reactants.

The effective core potential with scalar relativistic corrections (SBKJC) (Ref. 22) augmented by one set of *f* polarization functions (exponent=0.89) and one *s* and one set of *p* diffuse functions (exponent=0.01) was used on gold atoms, with the $5s^25p^65d^{10}6s^1$ electrons treated explicitly. Oxygen and hydrogen atoms employed the 6-31++G(*d*,*p*) basis set.[23] Spherical harmonic basis functions were used. The general atomic and molecular electronic structure system (GAMESS) program suite[24] was used in all the calculations and molecules were visualized with MACMOIPIT.[25]

## RESULTS AND DISCUSSION

The optimized structures and highest occupied molecular orbitals (MOs) of $Au_3$, $H_2O_2$, $O_2$, and $H_2$ are shown in Fig. 1. The $Au_3$ global minimum has $C_{2v}$ symmetry with a $^2B_2$ ground state, in accordance with experiment.[26] The three $Au_3$ MOs that arise from linear combinations of Au 6*s* atomic orbitals are also illustrated in Fig. 1. These are the bonding highest occupied MO (HOMO), the nonbonding singly occupied MO (SOMO) and the lowest unoccupied MO. The $O_2$ $D_{\infty h}$ ground term is $^3\Sigma_g^-$. This term corresponds to $^3B_{1g}$ in $D_{2h}$, which was used in the calculations.

The minima located on the $Au_3O_2$ potential energy surface (PES) are reported in Fig. 2. There are two possible ways in which $O_2$ can bind to $Au_3$. One is an "end-on" structure in which binding occurs through one oxygen and one gold atom. This structure belongs to $C_s$ symmetry and both terms $^2A'$ [Fig. 2(a)] and $^2A''$ [Fig. 2(b)] were found, with $^2A''$ being lower in energy. $O_2$ can also bind in a bridging manner. In this $C_{2v}$ arrangement, two oxygen atoms bind to two gold atoms forming a four-member ring. Three bridging minima, corresponding to $^2A_1$ [Fig. 2(c)], $^2B_2$ [Fig. 2(d)], and $^2A_2$ [Fig. 2(e)], have been found, with $^2A_2$ being the ground state term. The predicted global minimum with $O_2$ bridging between two Au atoms is in accordance with most recent published theoretical work,[10,11] while older studies reported the end-on structure to be the global minimum.[12,27,28] Some studies used the end-on species as the reactant rather than the global minimum bridging structure.[29]

Table I lists the binding energies at 0 K with and without ZPE corrections. The latter makes a small contribution in most cases. The ZAPT level of theory predicts that $O_2$ binds to $Au_3$ with a binding energy of ~8.5 kcal/mol, while the CCL binding energy is a much larger 14.5 kcal/mol. Previous DFT studies predict $Au_3$–$O_2$ binding energies of 7,[10] 5.8–16.1,[27] 15.2,[28] and 20.8 kcal/mol.[11] All of these calculations predict that $O_2$ will bind to $Au_3$. It is likely that CCL provides the most accurate prediction.

Now, consider the $Au_3$–$O_2$ interaction in greater detail. $O_2$ is a ground state triplet diradical with two degenerate singly occupied $\pi^*$ orbitals. In $C_{2v}$ symmetry these two $\pi^*$ orbitals of $O_2$ exhibit $b_2$ and $a_2$ symmetries. $Au_3$ has an unpaired electron located in the $\sigma$ nonbonding orbital with $b_2$ symmetry (see Fig. 1). Binding of $O_2$ to $Au_3$ occurs by the pairing of the unpaired electron in the $Au_3$ $b_2$ orbital with an unpaired electron in the $O_2$ $\pi^*$ $b_2$ orbital. This leads to the

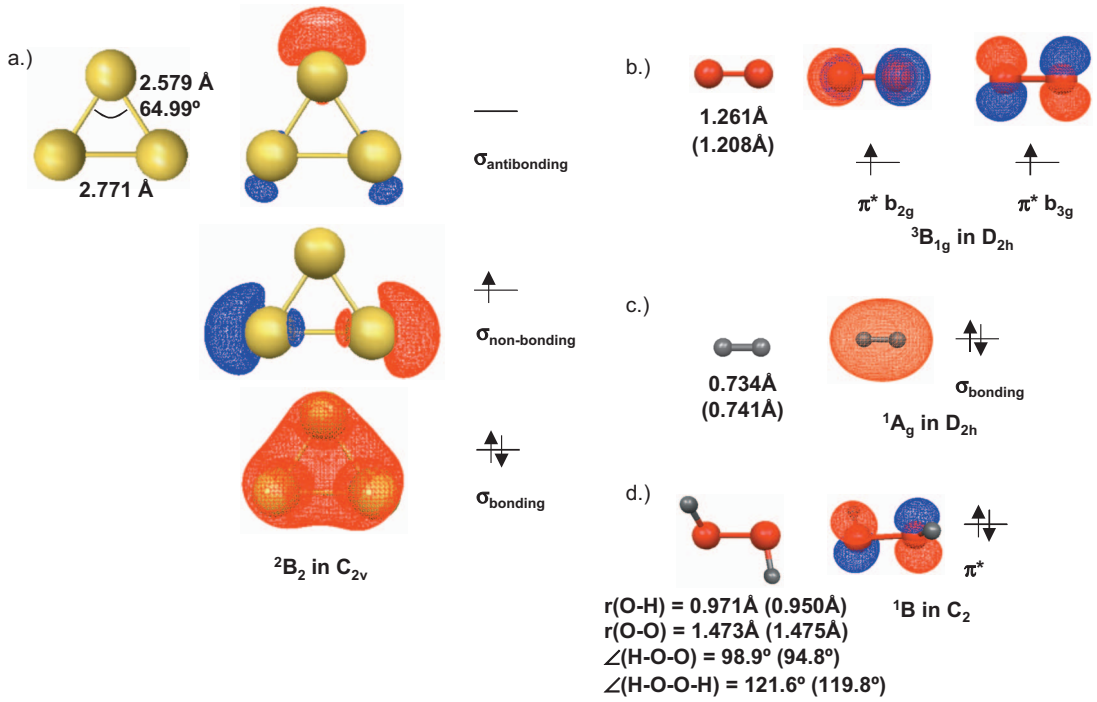


FIG. 1. (Color) ZAPT optimized geometries of (a) $Au_3$, (b) $O_2$, (c) $H_2$, and (d) $H_2O_2$. The $^3\Sigma_g^-$ in $D_{\infty h}$ corresponds to $^3B_{1g}$ in $D_{2h}$ for $O_2$. On the right of the structures all three $\sigma$ orbitals are shown for $Au_3$, and for the rest of the molecules the HOMOs are shown. Experimental data (Ref. 30) are given in parentheses.

formation of the $Au_3O_2$ global minimum, leaving the remaining unpaired electron in the $a_2$ $\pi^*$ orbital, yielding the ground state term.

Starting from the $Au_3O_2$ global minimum, $H_2$ was positioned ~5 Å away, and geometry optimization was performed in $C_s$ symmetry. No intervening barrier was found to prevent the binding of $H_2$ to $Au_3O_2$ to form $H_2Au_3O_2$. The latter species is the starting structure (reactant) presented as the first minimum (min1, the first point along the $x$-axis) in Fig. 3. This figure depicts the reaction coordinate diagram for the formation of $H_2O_2$ catalyzed by $Au_3$. As reported in Table I, at the ZAPT level of theory, $H_2$ binds to $Au_3$ by

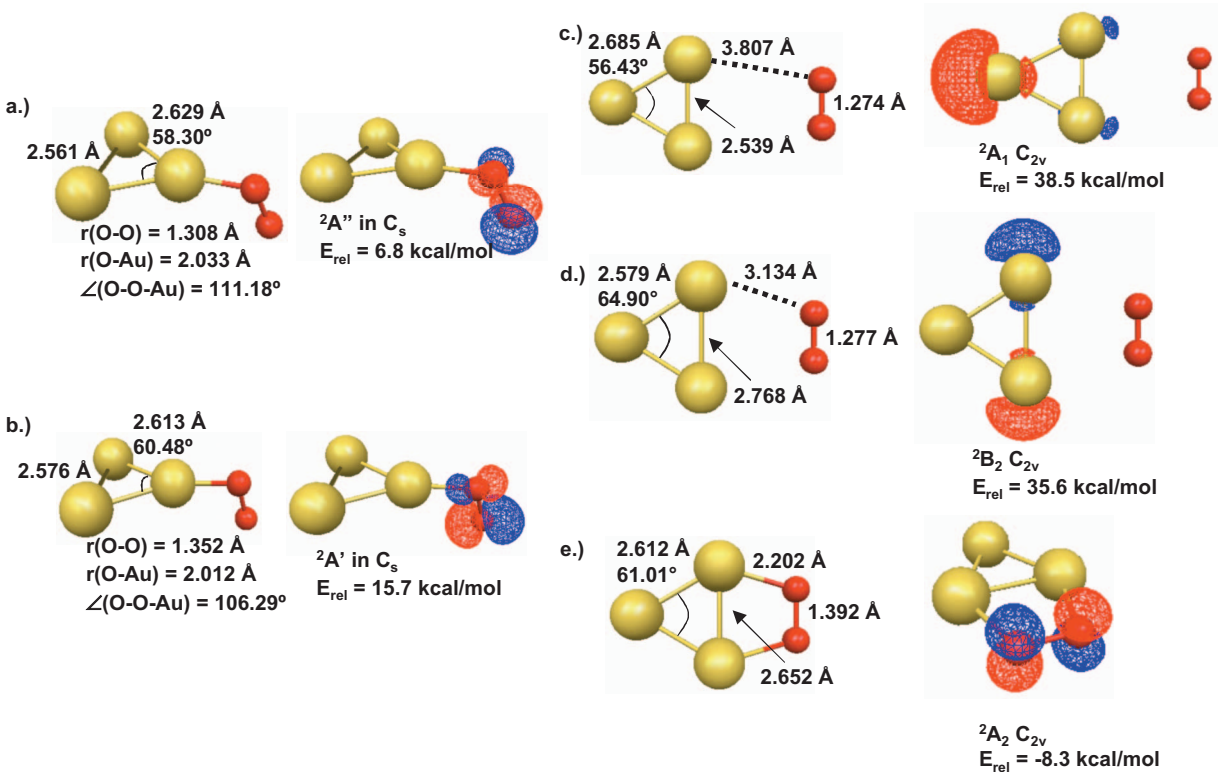


FIG. 2. (Color) ZAPT geometries of $O_2$ bound to $Au_3$ in $C_s$ symmetry. The geometric parameters are given on the left, while the term and corresponding highest SOMO are given on the right, with the relative energy with respect to the energy of separate species, $Au_3+O_2$.

TABLE I. ZAPT and CCL binding energies ($\Delta E_{bind}$) at 0 K, with and without ZPE corrections. The negative values indicate binding.

| | $\Delta E_{bind}$ (kcal/mol) | | | |
|---|---|---|---|---|
| Binding of | ZAPT | ZAPT+ZPE | CCL | CCL+ZPE |
| $O_2$ to $Au_3$ | −8.3 | −8.5 | −14.5 | −14.7 |
| $H_2$ to $Au_3O_2$ | −7.5 | −4.7 | −1.7 | 1.0 |
| $H_2O_2$ to $Au_3$ | −15.6 | −15.7 | −12.9 | −13.0 |
| $O_2$ to $Au_3H_2O_2$ | −2.6 | −1.8 | | |

7.5 (4.7) without (with) the ZPE correction. The CCL binding energy, in contrast, is very small. Indeed CCL with the ZPE correction predicts the addition of $H_2$ to $Au_3O_2$ to be slightly endothermic. Since the structures were not optimized at the coupled cluster level of theory and since anharmonicity and coupling of the vibrations were not taken into account, the addition of $H_2$ to $Au_3O_2$ could be either weakly exothermic or weakly endothermic.

Now consider (Fig. 3) the ZAPT reaction mechanism at 0 K, disregarding ZPE and thermal corrections. The starting structure (Fig. 3, min1) has both $O_2$ and $H_2$ bound to the $Au_3$ cluster. The reaction starts by breaking the H–H bond and transferring the first hydrogen atom to $O_2$ to form a hydroperoxide intermediate. This step, which proceeds in $C_s$ symmetry, must surmount a 9.4 kcal/mol barrier.

The attempt to locate the next transition structure (Fig. 3, TS2-3) was unsuccessful due to convergence problems in this region of the restricted open shell Hartree–Fock/ZAPT PES and possibly due to some configurational mixing. Thus, points along the ZAPT LLM path were employed to simulate this part of the reaction path, and the point with the highest energy on the LLM path is taken to be the approximate transition state (TS) for this step. The corresponding energy "barrier" of 3.5 kcal/mol is an upper limit to the actual barrier at the true transition state. Based on this small barrier, there may be some residual weak binding between the $HO_2$ hydrogen and the adjacent gold atom. On the other hand, CCL single points along this path suggest that there is no barrier at all in this region (i.e., TS2-3) of the reaction path.

The next two steps on the reaction path involve rearrangements of the $HO_2$ species, in order to attain an arrangement that is convenient for the ultimate formation of $H_2O_2$. These two steps proceed through ZAPT barriers of 9.1 (Fig. 3, TS3-4) and 2.2 (Fig. 3, TS4-5) kcal/mol. The second hydrogen atom then undergoes a 1,2-shift from one Au atom to form a Au–H–Au bridge. The ZAPT barrier for this step (Fig. 3, TS5-6) is 7.9 kcal/mol. This is followed by a repositioning of $HO_2$ with a small $\leqslant$2.4 kcal/mol barrier (Fig. 3, TS6-7), determined by following the corresponding LLM path.

The last two steps on the reaction path involve the completion of the transfer of the bridging H to the Au atom on which the $HO_2$ moiety resides, with a relatively low barrier of 4.6 kcal/mol (Fig. 3, TS7-8), and then the formation of $H_2O_2$ via a 7.6 kcal/mol barrier (Fig. 3, TS8-9).

The ZAPT and CCL reaction paths shown in Fig. 3 are in qualitative agreement with each other. These findings may be compared with a previous DFT study,[10] which reports a very small 2.2 kcal barrier for the formation of $HO_2$. This DFT study also predicts that the rate-controlling step in the epoxidation reaction is the actual epoxidation of propene with an activation barrier of 19.6 kcal/mol, rather than the formation of the hydroperoxide intermediate. A second DFT study by the same authors on the formation of $H_2O_2$ from $H_2$ and $O_2$ over $Au_3$ (Ref. 29) predicts the desorption of $H_2O_2$ to

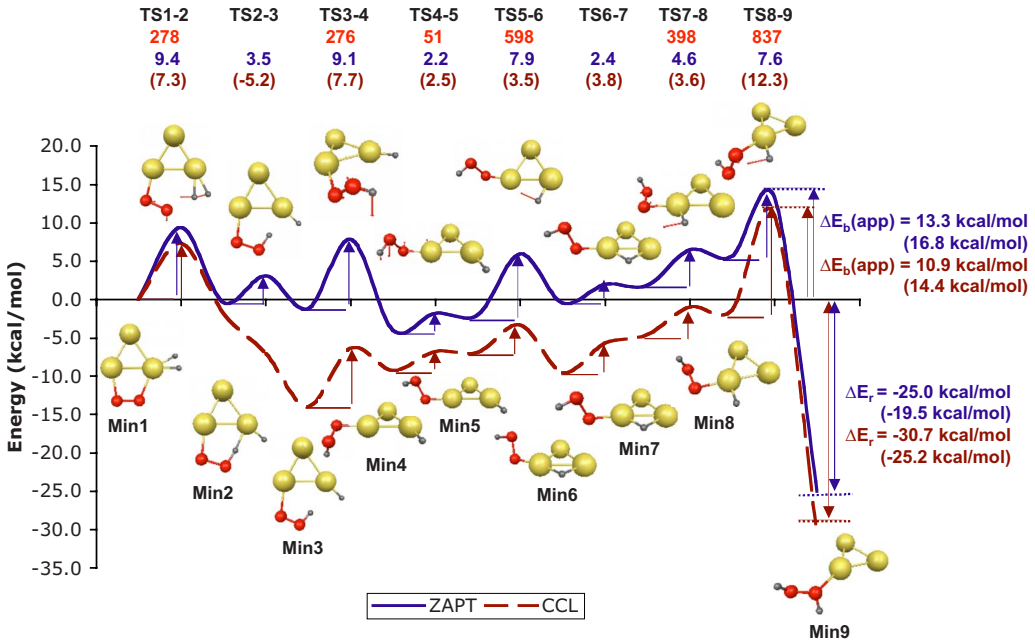


FIG. 3. (Color online) Reaction coordinate diagram of $H_2O_2$ formation from gaseous molecular $O_2$ and $H_2$ catalyzed by $Au_3$. Minima (min) are given below the reaction curve, while transition states (TS) are pictured above it. The corresponding imaginary frequency in $cm^{-1}$ is given first, followed by the ZAPT energy barrier and the CCL energy barrier (in parentheses), in kcal/mol, followed by the geometry of the depicted transition state. The ZAPT and CCL apparent energy barriers [$\Delta E_b$(app)] and reaction energies ($\Delta E_r$) are also provided, while activation energies and reaction enthalpies at 0 K are given in parentheses.

TABLE II. ZAPT and CCL activation energies ($\Delta E_a$), at 0 and 475 K, for each forward step of the reaction (see Fig. 3). TS(2) and TS(6) correspond to transition states that were estimated rather than located, so no Hessians are available at these points. The apparent energy of activation [$\Delta E_b$(app)] and reaction enthalpy ($\Delta H_r$) are reported as well.

| Structure | $\Delta E_a$ (ZAPT) (0 K) | $\Delta E_a$ (ZAPT) (425 K) | $\Delta E_a$ (CCL) (0 K) | $\Delta E_a$ (CCL) (425 K) |
|---|---|---|---|---|
| TS(1) | 9.2 | 8.9 | 7.2 | 6.8 |
| TS(3) | 8.2 | 8.4 | 6.8 | 6.9 |
| TS(4) | 0.2 | −0.3 | 0.5 | 0.0 |
| TS(5) | 6.5 | 6.5 | 2.1 | 2.1 |
| TS(7) | 4.5 | 4.0 | 3.5 | 3.0 |
| TS(8) | 8.4 | 8.0 | 13.1 | 12.7 |
| $\Delta E_a$ (app) (kcal/mol) | 16.8 | 16.3 | 14.4 | 14.0 |
| $\Delta H_r$ (kcal/mol) | −19.5 | −21.9 | −25.2 | −27.6 |

have the largest barrier (8.6 kcal/mol) for the reaction mechanism that is illustrated in Fig. 3. So, the DFT predicted highest point on the reaction path shown in Fig. 3 is roughly half that predicted by CCL, presumably the most reliable level of theory.

The calculated activation energies ($\Delta E_a$) and apparent energies of activation [$\Delta E_a$(app)] are listed in Table II. The rate-controlling step is the last step of the reaction that leads to the formation of $H_2O_2$. The most accurate (CCL) calculation gives $\Delta E_a$(app)=14.0 kcal/mol with both ZPE and thermal corrections at 425 K included. Note also that a CCL activation energy of almost 7 kcal/mol is needed for the formation of $HO_2$. The most accurate (CCL) calculation predicts $\Delta H_r$(425 K)=−27.6 kcal/mol. Inclusion of ZPE decreases, while the thermal correction increases the amount of released energy.

Selected minima are shown in Fig. 4 with emphasis on some geometrical parameters of interest and on the highest MO. Bond lengths and angles are chosen to illustrate important changes throughout the course of the reaction. Atoms are labeled and numbered as shown on the first structure.

It is informative to follow the electron density distribution of the unpaired electron, as depicted in Fig. 4 using Mulliken populations in the SOMOs. The reaction starts with the unpaired electron on $Au_3$ and a pair of unpaired electrons on $O_2$. Upon binding of $O_2$ to $Au_3$, the unpaired electron localizes mostly in the pair of $O_2$ $\pi^*$ orbitals, as shown by the Mulliken spin populations of ~0.5 on each of the oxygen atoms [Fig. 4(a)]. As the reaction progresses this electron density becomes somewhat delocalized, as shown in the spin populations on min4 in Fig. 4(b). Here, electron density is distributed among mostly gold atoms, which have atomic spin population ranging from 0.17 to 0.34. Somewhat lower Mulliken populations are found on the two H (~0.1) and two O (~0.1) atoms [Fig. 4(b)]. However, in the product, the unpaired electron density localizes in the nonbonding $Au_3$ $\sigma$

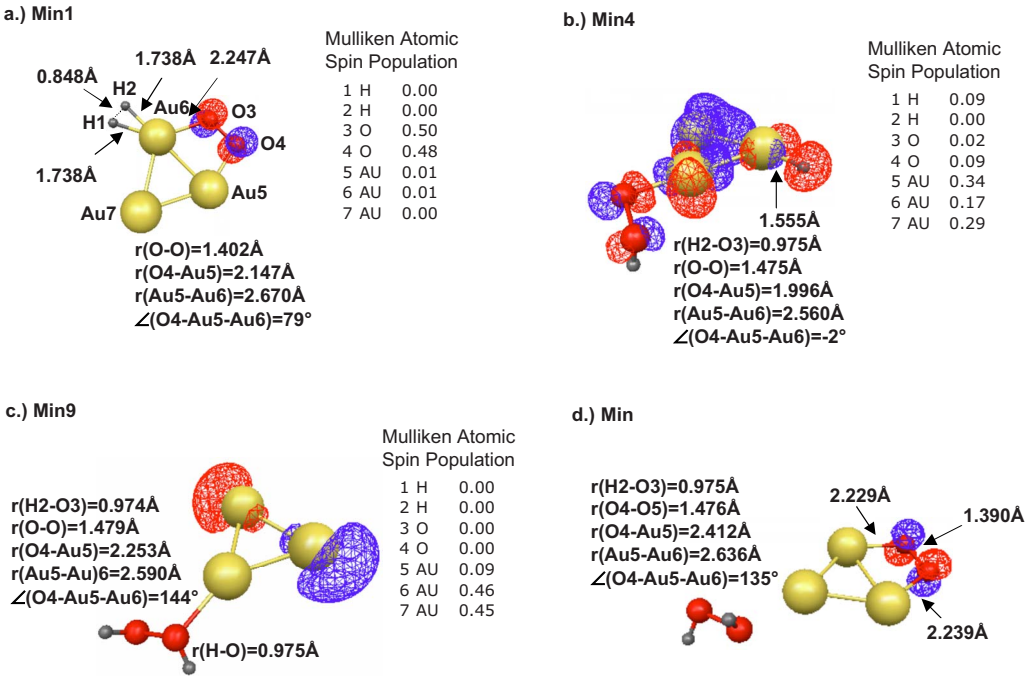


FIG. 4. (Color online) Depicted are the HOMO and some geometrical parameters. [(a)–(c)] Selected minima with the same numberings as in Fig. 3; the Mulliken atomic spin population is given on the right of the structures. (d) Minimum obtained upon binding of the second $O_2$ molecule to already formed $Au_3H_2O_2$. Atoms are numbered as shown on the first structure.

orbital, with atomic spin populations of ~0.45 on both $Au_6$ and $Au_7$ [Fig. 4(c)]. This $Au_3$ orbital is involved in the binding of $O_2$ to $Au_3$, so the catalytic cycle can proceed through the binding of the next $O_2$ molecule and simultaneous desorption of the formed $H_2O_2$ from $Au_3$ [Fig. 4(d)].

## CONCLUSIONS

A reaction mechanism for gas phase formation of $H_2O_2$ from $H_2$ and $O_2$ catalyzed by $Au_3$ is proposed. The catalytic activity of gold is achieved by activation of both $O_2$ and $H_2$ by weakening the O–O and H–H bonds. In addition, transfer of two hydrogen atoms to form first $HO_2$ radical and subsequently the molecule $H_2O_2$ is realized in a cascade of steps, each having a relatively low energy of activation. The most accurate calculations with ZPE and thermal corrections at 425 K included predict the final step of the reaction to be rate controlling. The apparent energy of activation is 14.0 kcal/mol, although it is important to note that the formation of $HO_2$ does require overcoming a barrier of almost 7 kcal/mol. The reaction is predicted to be highly exothermic by 27.6 kcal/mol.

## ACKNOWLEDGMENTS

This work was supported by grants from the Air Force Office of Scientific Research. The authors are grateful to Dr. Michael Schmidt and Dr. Ryan Olson, and to Professor Takako Kudo, Professor Keiji Morokuma, and Professor Lyudmila Slipchenko for enlightening discussions.

[1] Kirk-Othmer, *Kirk-Othmer Concise Encyclopedia of Chemical Technology*, 5th ed. (Wiley-Interscience, Hoboken, 2007).
[2] M. Haruta, T. Kobayashi, H. Sano, and N. Yamada, Chem. Lett. **1987**, 405.
[3] Y. A. Kalvachev, T. Hayashi, S. Tsubota, and M. Haruta, J. Catal. **186**(1), 228 (1999).
[4] "BASF, Dow, Solvay partnership breaks new ground with innovative HPPO technology in Antwerp," published online September 27, 2006, see http://www.corporate.basf.com/en/investor/news/mitteilunqen/pm.htm?pmid=2444&id=6ZLRUBxn_bcp.4k.
[5] B. K. Min and C. M. Friend, Chem. Rev. (Washington, D.C.) **107**, 2709 (2007).
[6] M. G. Clerici, G. Bellussi, and U. Romano, J. Catal. **129**, 159 (1991).
[7] P. Landon, P. J. Collier, A. J. Papworth, C. J. Kiely, and G. J. Hutchings, Chem. Commun. (Cambridge) **2002**, 2058; M. Okumura, Y. Kitagawa, K. Yamagcuhi, T. Akita, S. Tsubota, and M. Haruta, Chem. Lett. **2003**, 822.
[8] C. Sivadinarayana, T. V. Choudhary, L. L. Daemen, J. Eckert, and D. W. Goodman, J. Am. Chem. Soc. **126**, 38 (2004).
[9] T. A. Nijhuis, T. Q. Gardner, and B. M. Weckhuysen, J. Catal. **236**, 153 (2005).
[10] A. M. Joshi, W. N. Delgass, and K. T. Thomson, J. Phys. Chem. B **110**, 2572 (2006).
[11] G. Mills, M. S. Gordon, and H. Metiu, Chem. Phys. Lett. **359**, 493 (2002).
[12] S. A. Varganov, R. M. Olson, M. S. Gordon, and H. Metiu, J. Chem. Phys. **119**, 2531 (2003).
[13] S. A. Varganov, R. M. Olson, M. S. Gordon, G. Mills, and H. Metiu, J. Chem. Phys. **120**, 5169 (2004).
[14] J. Baker, J. Comput. Chem. **7**, 385 (1986); P. Culot, G. Dive, V. H. Nguyen, and J. M. Ghuysen, Theor. Chim. Acta **82**, 189 (1992); T. Helgaker, Chem. Phys. Lett. **182**, 503 (1991).
[15] T. Takada, M. Dupuis, and H. F. King, J. Chem. Phys. **75**, 332 (1981); W. D. Gwinn, *ibid.* **55**, 477 (1971).
[16] C. Gonzalez and H. B. Schlegel, J. Chem. Phys. **90**, 2154 (1989); M. W. Schmidt, M. S. Gordon, and M. Dupuis, J. Am. Chem. Soc. **107**, 2585 (1985); K. Ishida, K. Morokuma, and A. Komornicki, J. Chem. Phys. **66**, 2153 (1977); K. K. Baldridge, M. S. Gordon, R. Steckler, and D. G. Truhlar, J. Phys. Chem. **93**, 5107 (1989); B. C. Garrett, M. J. Redmon, R. Steckler, D. G. Truhlar, K. K. Baldridge, D. Bartol, M. W. Schmidt, and M. S. Gordon, *ibid.* **92**, 1476 (1988).
[17] T. J. Lee, A. P. Rendell, K. G. Dyall, and D. Jayatilaka, J. Chem. Phys. **100**, 7400 (1994); T. J. Lee and D. Jayatilaka, Chem. Phys. Lett. **201**, 1 (1993).
[18] G. D. Fletcher, M. S. Gordon, and R. S. Bell, Theor. Chem. Acc. **107**, 57 (2002); C. M. Aikens, G. D. Fletcher, M. W. Schmidt, and M. S. Gordon, J. Chem. Phys. **124**, 014107 (2006).
[19] M. Wloch, J. R. Gour, and P. Piecuch, J. Phys. Chem. A **111**, 11359 (2007); P. Piecuch and M. Wloch, J. Chem. Phys. **123**, 224105 (2005).
[20] Y. Ge, M. S. Gordon, and P. Piecuch, J. Chem. Phys. **127**, 174106 (2007).
[21] A. K. Sinha, S. Seelan, M. Okumura, T. Akita, S. Tsubota, and M. Haruta, J. Phys. Chem. B **109**, 3956 (2005).
[22] W. J. Stevens, M. Krauss, H. Basch, and P. G. Jasien, Can. J. Chem. **70**, 612 (1992).
[23] W. J. Hehre, R. Ditchfield, and J. A. Pople, J. Chem. Phys. **56**, 2257 (1972).
[24] M. W. Schmidt, K. K. Baldridge, J. A. Boatz, S. T. Elbert, M. S. Gordon, J. H. Jensen, S. Koseki, N. Matsunaga, K. A. Nguyen, S. Su, T. L. Windus, M. Dupuis, and J. A. Montgomery, Jr., J. Comput. Chem. **14**, 1347 (1993); M. S. Gordon and M. W. Schmidt, *Theory and Applications of Computational Chemistry: The First Forty Years* (Elsevier, Amsterdam,. The Netherlands, 2005), p. 1167.
[25] B. M. Bode and M. S. Gordon, J. Mol. Graphics Modell. **16**, 133 (1998).
[26] J. A. Howard, R. Sutcliffe, and B. Mile, J. Chem. Soc., Chem. Commun. **1983**, 1449.
[27] X. Ding, Z. Li, J. Yang, J. G. Hou, and Q. Zhu, J. Chem. Phys. **120**, 9594 (2004).
[28] B. Yoon, H. Haekkinen, and U. Landman, J. Phys. Chem. A **107**, 4066 (2003).
[29] D. H. Wells, W. N. Delgass, and K. T. Thomson, J. Catal. **225**, 69 (2004).
[30] D. J. I. Russell, NIST Computational Chemistry Comparison and Benchmark Database, NIST Standard Reference Database Number 101 (2005).